International Journal of Mass Spectrometry 365–366 (2014) 68–74

Contents lists available at ScienceDirect

International Journal of Mass Spectrometry

journal homepage: www.elsevier.com/locate/ijms

Bond-forming reactions between the molecular oxygen dication and small organic molecules☆

Michael A. Parkes*, Jessica F. Lockyear[1], Stephen D. Price**

University College London, Department of Chemistry, 20 Gordon Street, London WC1H 0AJ, United Kingdom

ARTICLE INFO

Article history:
Received 5 November 2013
Received in revised form 20 January 2014
Accepted 21 January 2014
Available online 30 January 2014

Keywords:
Dications
Ion chemistry
Coincidence techniques
Time of flight mass spectrometry

ABSTRACT

The reactions of O_2^{2+} with CH_4, C_2H_2 and C_2H_4 have been investigated for the first time, using a position-sensitive coincidence technique, at centre-of-mass collision energies close to 4 eV. The experiments show these interactions yield a wide variety of products which involve the formation of new chemical bonds. The mechanisms of these bond-forming reactions have been investigated by examining the correlations between the velocities of the reactant and product ions which are revealed by the coincidence data. Many of the bond-forming reactions occur *via* the stripping of an atom (or group of atoms) from the neutral by the O_2^{2+} reactant, while other reactions clearly involve the initial formation of a collision complex which then fragments to form the detected products.

1. Introduction

From a fundamental viewpoint O_2^{2+} is one of the simplest molecular dications. Establishing a detailed understanding of the reactivity of O_2^{2+} is therefore an important step towards predicting and accounting for the reactivity of larger dications. The O_2^{2+} ion is expected to be present in the Earth's upper atmosphere [1–3] and reports of ionospheric modelling have concluded that "doubly-charged ions are a common feature of planets and satellites with thick atmospheres". Given the potential atmospheric importance of O_2^{2+}, we have begun a series of investigations of the reactions of O_2^{2+} with a variety of small neutral species [4,5]. In this paper we report the first study of the reactions of the molecular oxygen dication with three simple organic molecules methane (CH_4), ethyne (C_2H_2) and ethene (C_2H_4). These investigations were performed using a coincidence technique that, as well as identifying the reaction products, probes the dynamics of product formation in these dication-neutral reactions.

Little attention has been paid to the bimolecular reactivity of O_2^{2+} [5–7]. However, the reactions of dications with small organic molecules have been previously investigated, with particular attention paid to reactions with methane. The reactions of CH_4 with Ar^{2+} have been studied using a variety of techniques, with one study employing a Selected Ion Flow Tube (SIFT) and a Selected Ion Drift Tube (SIDT) [8,9]. In this work Störi et al. found that the only reaction between Ar^{2+} and CH_4 was single electron transfer occurring at the collisional rate, a finding confirmed by Franceschi et al. [10]. The reaction of Ar^{2+} with C_2H_2 has also been studied using a SIDT, with the results suggesting that the collisions again result in electron transfer at the collisional rate [8,11]. We have previously studied the reaction of $Ar^{2+} + C_2H_2$ using our position sensitive coincidence (PSCO) spectrometer, the same apparatus that we employ for the studies reported in this paper [12]. Our study of the Ar^{2+}/C_2H_2 collision system revealed that, although electron transfer was the major reaction pathway, there was also a bond-forming channel producing ArC^+. Roithová and Schröder and others have examined how a large number of organic dications react with CH_4 [13–16], finding that the major reaction channels were again due to electron transfer. However, Roithová and Schröder also detected a large number of bond-forming reactions, including processes in which new carbon–carbon bonds were formed [14–16]. Other groups have observed that atomic transition metal dications (M) will react with CH_4 to generate products of the form MCH_2^{2+} [17–22]. Indeed, it was recently discovered that analogous MCH_2^{2+} products are formed following the reaction of Th^{2+} and CH_4 but that no reaction occurs between U^{2+} and CH_4 [23].

When a dication and neutral react in the gas-phase there are three general classes of pathway that can be followed: single

* Corresponding author.
** Corresponding author. Tel.: +44 2076794606.
E-mail addresses: michael.parkes@ucl.ac.uk (M.A. Parkes), s.d.price@ucl.ac.uk (S.D. Price).
[1] Current address: Lawrence Berkeley National Laboratories, 1 Cyclotron Road, Berkeley, CA 94720, USA.

1387-3806/$ – see front matter © 2014 The Authors. Published by Elsevier B.V. All rights reserved.
http://dx.doi.org/10.1016/j.ijms.2014.01.014

electron transfer (SET), double electron transfer (DET) and bond-forming reactions. In both SET and DET electrons are transferred from the neutral species to the reactant dication. Dicationic electron transfer reactivity is now fairly well understood [12,24–28], and hence this paper will focus on documenting and explaining the bond-forming reactions that occur between O_2^{2+} and CH_4, C_2H_2 and C_2H_4 at low collision energies in the centre-of-mass (CM) frame. As mentioned above, these reactions have been studied using an experiment that involves the coincident detection of product ion pairs from individual dicationic reactive events, at a position-sensitive detector. This experimental methodology both identifies the different reactive channels resulting from the dication-neutral encounters and reveals the detailed kinematics of these reactive processes [29–31].

2. Experimental and data analysis

2.1. PSCO apparatus

The details of the PSCO experiment have been presented in the literature before [30,31]. In brief, ions are generated from a precursor gas by electron ionisation in a home-built ion source. The positive ions formed in the source are extracted and focussed onto the entrance slit of a hemispherical analyser. The ions are energy selected by the analyser to produce an ion beam with an energy spread of approximately 0.3 eV. This ion beam is swept across an aperture, to form ion pulses, before entering a commercial velocity filter. The velocity filter is set to pass only ions with the required mass-to-charge ratio; in the studies reported here this ratio was 16. The resulting mass and energy selected ion beam is then decelerated to the chosen laboratory-frame collision energy before entering the interaction region of the spectrometer.

In the interaction region of the apparatus, the mass-selected beam of ions crosses an effusive jet of the neutral reagent, and dication-neutral collisions occur under single-collision conditions. The interaction region also doubles as the source region of a time-of-flight mass spectrometer (TOFMS) and, once the pulse of dications has interacted with the neutrals, a positive voltage is applied to a repeller plate to start the mass-spectral acquisition. This positive potential forces any cations in the interaction region into the acceleration region of the TOFMS and then into a field-free flight-tube. The axis of the TOFMS is oriented parallel to the direction of the reactant dication beam and the spectrometer is designed to implement second-order space focussing [32]. At the end of the flight tube ions are detected by a position sensitive detector with a dual delay-line anode [33]. The detector's output allows access to an ion's arrival time and the position (x, y) of that ion's impact on the detector face. Signals from the detector are amplified and discriminated before being passed to a PC based time-to-digital convertor. If two ions are detected in the same TOFMS cycle then they are recorded as a coincidence event and each ion's arrival time and impact position on the detector are stored for off-line analysis.

As discussed before, the conditions under which the experiment operates, for example the intensity of the dication beam, are carefully chosen to minimise the rate of false coincidences [34]. However, despite these efforts, the presence of a significant number of O^+ ions accompanying the O_2^{2+} ions in the ion beam raises the false coincidence rate for dication reactions generating a product at $m/z = 16$. These increased false coincidence rates are dramatically reduced, at little cost to the number of true coincidences, by excluding a narrow range of flight times close to $m/z = 16$ [34].

2.2. Data analysis

To analyse the data recorded using the PSCO experiment, at a given collision energy, we generate a two-dimensional histogram (a pairs spectrum) of the arrival times of the pairs of ions detected in coincidence. Different reaction channels produce distinct and discrete peaks in this pairs spectrum. The groups of ion pair events that make up each of the different peaks in the pairs spectrum are then selected, in turn, for further analysis. For a given set of selected ion pairs, a set which characterises a single reactive channel, the timing and positional information is used to determine the x, y and z velocity vectors of the product ions in the CM frame, $w(X^+)$ and $w(Y^+)$. The details of this transformation have been presented before [30,31]. For three-body reactions, in which a neutral fragment is formed along with two product ions, the CM velocity of the neutral can be determined from the velocities of the accompanying two ions using conservation of momentum. This extraction of the velocities of the neutral species accompanying ion pair formation allows a detailed insight into the kinematics of three-body dicationic reactions [30,31]. Following the determination of the product velocities, the relationship between these vectors can be examined to reveal any correlations between their motions, a powerful probe of the reaction mechanism [12,29,34].

Two different classes of scattering diagram are used to reveal the correlations between the product velocities [30,31]. Both diagrams are polar histograms in which the radial coordinate is the magnitude of the CM velocity of a product (*e.g.* $|w(X^+)|$ for product ion X^+) while the angular coordinate is the angle between $|w(X^+)|$ and another velocity of the collision system. In the first class of diagram, a *CM scattering diagram*, the angle plotted is the angle between the product's velocity vector and the direction of the velocity of the CM of the collision system. In the second class of scattering diagram the angular coordinate is the angle of one product's CM velocity vector (*e.g.* X^+) relative to the CM velocity vector of a second product (*e.g.* Y^+). This second class of diagram is referred to as an *internal frame* scattering diagram [31]. Internal frame scattering diagrams are particularly valuable for the insight they provide concerning the reaction's dynamics. Since the scattering angles vary between 0° and 180°, the scattering data for one species can be plotted in the upper half of the diagram and the data for another species in the lower half.

The PSCO data for an individual reactive channel can also be used to determine the energetics of a given reaction channel. For the channel of interest, an average (or modal) value of the kinetic energy release T in the CM frame for the reaction can be calculated from the product velocities. The value of T can then be related to the translational exothermicity of a reaction (ΔE_T) using E_{com}, the CM collision energy of the reactive system [31,34]:

$$\Delta E_T = E_{prods} - E_{reacts} = T - E_{com} \quad (1)$$

In Eq. (1) the energies of the products and reactants (E_{prods} and E_{reacts}) include any internal energy of the products and reactants. If the products and reactants have no internal energy then $-\Delta E_T$ will be equal to the reaction enthalpy ($\Delta_r H$). If ΔE_T and the literature exothermicity of the reaction (ΔH_{lit}) are known then any differences between them reveals the internal excitation of the products and/or the reactants [35].

3. Results and discussion

3.1. $O_2^{2+} + CH_4$

Following the reaction of O_2^{2+} with CH_4 at $E_{com} = 4.0$ eV a number of different product channels are observed. The results given in Table 1 show that over 80% of the reactive collisions between

Table 1
Observed reaction channels, together with their branching ratios and enthalpies, following the reaction of O_2^{2+} with CH_4 at E_{com} = 4.0 eV. Relevant energetics are determined from literature values [39] coupled with the double ionisation energy of O_2 [42].

Channel	Products	Branching ratio	$-\Delta E_T$/eV	ΔH_{lit}/eV[a]
	Single electron transfer	83.7		
	Double electron transfer	8.8		
	Bond forming			
1.1	$HCO^+ + H^+ + [2H + O]$	3.3		−3.9[b]
1.2	$HCO^+ + H_2^+ + [O + H]$	2.4		−6.5[b]
1.3	$HCO^+ + H_3^+ + O$	0.1	−5.6	−12.7[b]
1.4	$HO_2^+ + CH_2^+ + H$	1.2	−7.0	−7.4
1.5	$HO_2^+ + CH^+ + [2H]$	0.3		−2.7
1.6	$CO_2^+ + H^+ + [3H]$	0.1		−3.0
1.7	$CO_2^+ + H_2^+ + [2H]$	0.1		−5.7

[a] All enthalpies are calculated assuming the neutral products are fully atomised.
[b] Enthalpy has been calculated assuming that the product is in the form HCO^+ not COH^+.

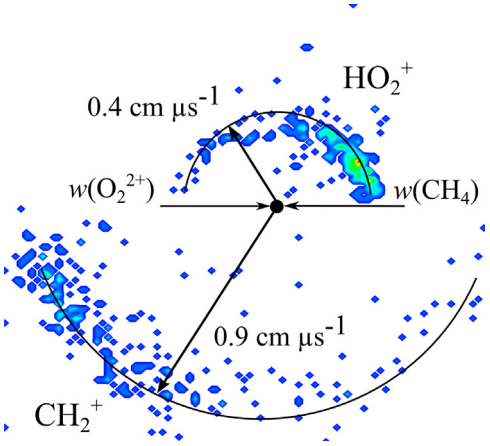

Fig. 1. The CM frame scattering diagram for the formation of $HO_2^+ + CH_2^+$ (channel 1.4) following the reaction of $O_2^{2+} + CH_4$ at E_{com} = 4.0 eV.

O_2^{2+} and CH_4 result in SET, while 9% result in DET. The remaining 7% of the reactive collisions result in formation of new chemical bonds between the reactants. The main product ion from these bond-forming reactions is HCO^+ which is accompanied by either H^+ (channel 1.1), H_2^+ (channel 1.2) or H_3^+ (channel 1.3). The next most abundant product ion from the bond-forming reactions is HO_2^+. This product ion is formed along with either CH_2^+ (channel 1.4) or CH^+ (channel 1.5). There are also two weak channels in which CO_2^+ is generated, accompanied by H^+ (channel 1.6) or H_2^+ (channel 1.7). As outlined above, the PSCO dataset not only reveals the branching ratios into each of the reaction channels, but it also can be used to probe the mechanisms of the bond-forming processes. In the following sections we discuss the mechanisms of these bond-forming reactions in turn.

3.1.1. Formation of HO_2^+

Fig. 1 shows the CM scattering diagram for HO_2^+ and CH_2^+ formed in channel 1.4 (Table 1). The CM scattering from channel 1.5 (formation of HO_2^+ and CH^+) is almost identical in form to the scattering illustrated in Fig. 1. Fig 1 shows that there is a strong anisotropy in the CM scattering of the products of channel 1.4; the HO_2^+ is strongly scattered in the direction of the CM velocity of the O_2^{2+} reactant, while the CH_2^+ is strongly scattered in the opposite direction, the direction of motion of the CH_4 reactant. This strong forward scattering shows that the formation of HO_2^+ and CH_2^+ occurs *via* a direct pathway, where the O_2^{2+} strips a hydride ion from the CH_4. As has been observed before, this stripping process does not significantly perturb the direction of the product velocities in relation to the velocities of the reactants [12,34]. As both channels 1.4 and 1.5 show essentially identical scattering, it seems clear that the same initial stripping process occurs in both cases, to form $HO_2^+ + CH_3^+$, and the nascent CH_3^{+*} then dissociates into $CH_2^+ + H$ (channel 1.4) or $CH^+ + [H + H]$ (channel 1.5); these hydrocarbon cations are then detected together with the HO_2^+. For channel 1.4 a modal $-\Delta E_T$ value of −7.0 eV is derived from our data. Comparison of this energy release to the ground-state literature value for the enthalpy of the reaction, −7.4 eV, shows that most of the energy released by the reaction goes into product translational energy and not into internal excitation.

3.1.2. Formation of HCO^+

The second set of bond-forming reactions we consider are those forming HCO^+ (Reactions 1.1–1.3). The CM scattering diagram for channel 1.1 (Fig. 2(a)) shows the HCO^+ and H^+ products are scattered fairly isotropically about the CM. This form of scattering indicates that the reaction proceeds *via* a collision complex that survives for several rotational periods [36]. When combined with similar CM scattering for channels 1.2 and 1.3, our data then clearly shows that the mechanism for HCO^+ formation from the O_2^{2+}/CH_4 collision system is always *via* a "long-lived" complex. As channel 1.3 is a three-body reaction, yielding $HCO^+ + H_3^+ + O$, we can examine the internal frame scattering of the products for this channel to provide more insight into the general reaction mechanism leading to HCO^+ formation. Fig. 2(b) shows the internal frame scattering of the HCO^+ and O products from channel 1.3 in the frame defined by the velocity of the H_3^+ product. Though this channel is weak, it is clear that HCO^+ and O are scattered about a point that is displaced by about 0.2 cm μs^{-1} from the CM. As has been discussed in detail before [4,37], this form of scattering indicates that the

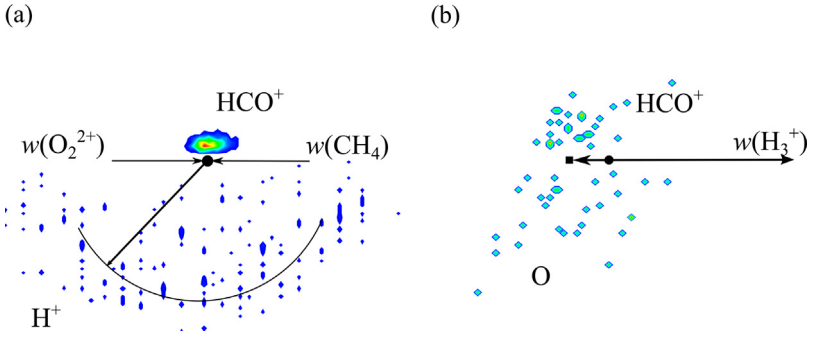

Fig. 2. Scattering diagrams recorded following the reaction of $O_2^{2+} + CH_4$ at E_{com} = 4.0 eV. (a) The CM frame scattering for the formation of the $HCO^+ + H^+$ products from channel 1.1. The arc marks a CM velocity of 3.0 cm μs^{-1}. (b) Internal frame scattering diagram for HCO^+ and O relative to H_3^+ for channel 1.3. The square marks the velocity of the dissociating precursor HCO_2^{+*} (0.2 cm μs^{-1}). The centre of mass is marked by the back dot at the centre of each diagram.

HCO^+ and O products originate from a nascent HCO_2^{+*} ion, formed in the primary dissociation of the $[O_2–CH_4]^{2+}$ collision complex. The velocities of the HCO^+ and O products, in the internal frame defined by H_3^+, will then be centred about a point displaced away from the CM by an amount equal to the CM velocity of the HCO_2^{+*} precursor. As $w(H_3^+)$ is known from our data, $w(HCO_2^{+*})$ can readily be estimated using conservation of momentum. From our data, the average value of $w(H_3^+)$ is measured to be 2.3 cm μs^{-1}, which leads to a value of 0.2 cm μs^{-1} for $w(HCO_2^{+*})$. This value is clearly in excellent agreement with the shift observed in Fig. 2(b), strongly supporting the sequential mechanism:

$$O_2^{2+} + CH_4 \rightarrow [O_2–CH_4]^{2+} \rightarrow HCO_2^+ + H_3^+ \rightarrow HCO^+ + O + H_3^+ \quad (2)$$

Alternative sequential mechanisms for this reaction (*e.g.* formation of H_3O^+) all lead to predicted precursor velocities which are markedly different from that observed in the data (Fig. 2b).

Formally, it is not possible to determine the neutral velocities associated with the two other product channels (1.1 and 1.2) that form HCO^+ in this collision system, as these reactions are potentially four-body processes. However, given the identity of the products in these three channels (1.1–1.3) it seems highly likely that they share a common first step: the formation of HCO_2^{+*} and H_3^+ as the primary fragments of the collision complex, with the HCO_2^{+*} going on to fragment to give HCO^+. The three different bond-forming channels then arise as the H_3^+ product can either remain intact (channel 1.3) or fragment to H_2^+ or H^+. From the energetics of reaction 1.3 it is clear that there is about 7 eV of internal energy distributed between the $HCO^+ + H_3^+ + O$ products ($-\Delta E_T = -5.6$ eV while $\Delta H_{lit} = -12.7$ eV). Such an internal energy is sufficient, if correctly distributed, to break the bonds in H_3^+ to form either $H^+ + H_2$ or $H_2^+ + H$.

3.1.3. Formation of CO_2^+

The final group of bond-forming reactions observed following collisions of O_2^{2+} and CH_4 involve the formation of CO_2^+, paired with either H^+ or H_2^+. Unfortunately, these channels are very weak and so it is not possible to construct statistically meaningful scattering diagrams from these data. We remark that the formation of products involving such an extensive rearrangement from the connectivity of the reactants most likley involves the formation of a long-lived complex between O_2^{2+} and CH_4.

3.1.4. Computational chemistry

In order to support the mechanistic conclusions derived above from our experimental data, we have performed a preliminary exploration of the $[O_2–CH_4]^{2+}$ potential energy surface using Gaussian 09 [38]. Stationary points were first located and characterised using an MP2/aug-cc-pVTZ methodology. The energies of these stationary points were then determined using a CCSD(T) algorithm with the same basis set. Zero-point energies were taken from the MP2 results. The stationary points we have located are shown in Fig. 3 with detailed geometries given in Supplementary Information. A bound $[O_2–CH_4]^{2+}$ collision complex exists on the potential energy surface, lying about 7 eV below the asymptotic energy of the reactants. A transition state was located that connects this collision complex to a rearranged geometry in which an H atom has migrated from the methane group to the terminal oxygen atom (Fig. 3). Loss of H_3^+ from this rearranged complex would leave a $[COOH]^+$ species, the same species we identified above as the precursor to the HCO^+ products we detect. This primary ion could also lose an H atom to act as the source of the CO_2^+ we detect in channels 1.6 and 1.7. Thus, the computational results support the conclusions on the reaction mechanisms drawn from the experimental data.

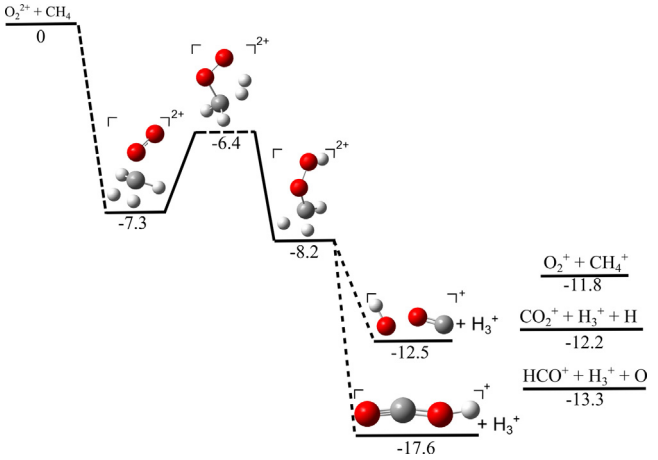

Fig. 3. Calculated stationary points on the $[O_2–CH_4]^{2+}$ potential energy surface and their relative energies in electronvolts. See text for details. A solid line connecting the stationary points indicates that an IRC calculation has confirmed their connectivity. Note, that the vertical energy scale is not continuous. Detailed geometries of the stationary points are given in the Supplementary Information.

3.2. $O_2^{2+} + C_2H_2$

Table 2 summarises the reactions we observe following collisions of O_2^{2+} with C_2H_2 at $E_{com} = 4.0$ eV. Similarly to the reaction of O_2^{2+} with CH_4, SET accounts for the vast majority (87%) of the product ion yield from the O_2^{2+}/C_2H_2 collision system, with bond-forming reactions contributing around 10%. Of the nine observed bond-forming channels, two involve the formation of HCO^+ (2.1 and 2.2), four the formation of CO^+ (2.3–2.6) and the remaining three channels (2.7–2.9) generate C_2OH^+, C_2O^+ and CO_2^+ respectively.

3.2.1. HCO^+ formation

The most intense bond-forming channel from the O_2^{2+}/C_2H_2 collision system is channel 2.1, which involves formation of $HCO^+ + CH^+ + O$. The formation of three products in this channel mean it is possible to use the PSCO data to reconstruct the complete velocity distribution for all the products. The CM scattering diagram for channel 2.1 is shown in Fig. 4(a) revealing scattering for the CH^+ product which is markedly anisotropic. The HCO^+ product also shows strong anisotropy (Fig. 4(a)), but with a more pronounced

Table 2
Observed reaction channels, together with their branching ratios and enthalpies, following the reaction of O_2^{2+} with C_2H_2 at $E_{com} = 4.0$ eV. Relevant energetics are determined from literature values [39] coupled with the double ionisation energy of O_2 [42].

Channel	Products	Branching ratio	$-\Delta E_T$/Ev	ΔH_{lit}/eV[a]
	Single electron transfer	87.4		
	Double electron transfer	2.6		
	Bond forming			
2.1	$HCO^+ + CH^+ + O$	5.5	−4.5	−10.5[b]
2.2	$HCO^+ + C^+ + [O + H]$	0.6		−6.4[b]
2.3	$CO^+ + H^+ + [C + H + O]$	0.4		2.5
2.4	$CO^+ + CH_2^+ + O$	1.3	−5.4	−8.7
2.5	$CO^+ + CH^+ + [O + H]$	1.7		−4.0
2.6	$CO^+ + C^+ + O + [2H]$	0.3		0.2
2.7	$C_2OH^+ + H^+ + O$	0.1		–[c]
2.8	$C_2O^+ + H^+ + [O + H]$	0.1		–[c]
2.9	$CO_2^+ + H^+ + [C + H]$	<0.1		−3.2

[a] All enthalpies are calculated assuming the neutral products are fully atomised.
[b] Enthalpy has been calculated assuming that the product is in the form HCO^+ not COH^+.
[c] No relevant enthalpies of formation are available.

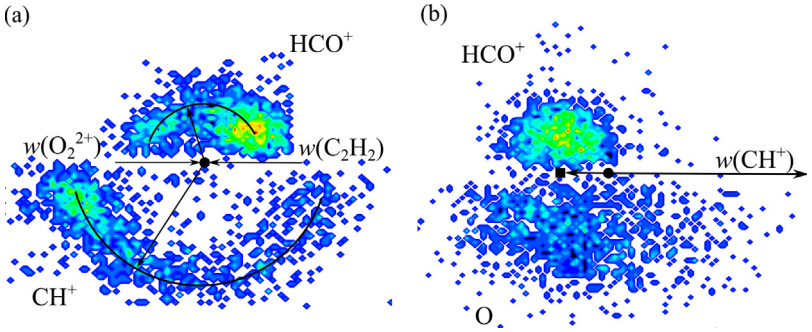

Fig. 4. Scattering diagrams for the reaction of $O_2^{2+} + C_2H_2$ at E_{com} = 4.0 eV. The black dot at the centre of the diagrams marks the CM. (a) The CM frame scattering diagram for the $HCO^+ + CH^+$ products from channel 2.1. The upper arc indicates a CM velocity of 0.4 cm μs^{-1} while the lower arc indicates a CM velocity of 1.0 cm μs^{-1}. (b) Internal frame scattering of HCO^+ and O relative to CH^+ for channel 2.1. The square marks the velocity of the dissociating precursor HCO_2^{+*} (0.4 cm μs^{-1}).

tail to larger scattering angles. The HCO^+ is predominantly scattered in the direction of motion of the O_2^{2+} reactant and the CH^+ product is scattered in the direction of motion of the C_2H_2 reactant. This scattering is, as has been discussed above, indicative of a direct reaction where the O_2^{2+} effectively extracts a CH^- from C_2H_2. The internal frame scattering of HCO^+ and O relative to CH^+ for this channel is shown in Fig. 4(b). In this diagram it is clear that both HCO^+ and O are scattered isotropically around a point that is displaced away from the CM, in the opposite direction to the velocity of the CH^+ product. As described above, this scattering pattern reveals that initial formation of $CHO_2^+ + CH^+$ is followed by ejection of O from CHO_2^+ to give the observed HCO^+ product. Further support for this mechanistic insight comes from the fact that the HCO^+ and O products are distributed about a point that is displaced 0.4 cm μs^{-1} away from the CM. This value is the same as the expected magnitude of the mean velocity of the dissociating CHO_2^{+*} precursor, calculated from the average velocity of the CH^+ product (1.2 cm μs^{-1}) *via* conservation of momentum

Comparing the values of ΔE_T and ΔH_{lit} for channel 2.1 indicates that there is around 6 eV of excess energy in the internal modes of the $HCO^+ + CH^+ + O$ products. Only 4.1 eV is required to fragment CH^+ into $C^+ + H$. Therefore, it seems very likely that the initial stripping step on the pathway to form $HCO^+ + CH^+$ (channel 2.1) also leads to the formation of the products in channel 2.2 ($HCO^+ + C^+$), with the CH^+ product now dissociating to give C^+ and H. At first glance, it is perhaps surprising that the strong C–C triple bond of C_2H_2 can be broken in a direct reaction, without the formation of a longer lived collision complex. However, previous studies of the reaction of Ar^{2+} with C_2H_2 have shown ArC^+ is formed *via* an exactly analogous direct transfer of a CH^- from C_2H_2 to Ar^{2+} [12].

3.2.2. Formation of CO^+

The second major product from bond-forming $O_2^{2+} + C_2H_2$ interactions is CO^+, a product ion which is involved in four reaction channels accompanied by either H^+, CH_2^+, CH^+ or C^+. Only in channel 2.5, where CO^+ is formed in conjunction with CH^+, is the signal level sufficient to extract meaningful scattering diagrams, and the CM scattering for this channel is shown in Fig. 5. Despite the weak signals the CM scattering in channel 2.5 appears broadly isotropic, extending over all scattering angles. Such scattering again suggests that the CO^+ is formed *via* an intermediate collision complex. Given that we commonly see such collision complexes undergo a primary fragmentation to a pair of nascent product ions that can subsequently fragment further, a viable mechanism for the formation of CO^+ involves the fragmentation of the collision complex into a pair of energetically excited ions: $CO_2^{+*} + CH_2^{+*}$. For the channels under discussion the nascent CO_2^+ fragments to form CO^+ which is detected in coincidence with CH_2^+ or the products of its decay (H^+, CH^+ or C^+). Further support fro this reaction pathway is that survival of the CO_2^+, accompanied by fragmentation of the CH_2^+ to H^+ yield us the products detected in Channel 2.9 (see below).

3.2.3. Other products

Three other ions, produced by bond-forming reactions, are also observed following the reaction of O_2^{2+} and C_2H_2. These products are C_2O^+, C_2OH^+ and CO_2^+ (Channels 2.7–2.9, Table 2). The signals from these channels are all too weak to allow any reliable analysis of their reaction dynamics. However, the formation of these ions involves major rearrangements in the connectivity of the reactants and points to the importance of a collision complex in the respective reaction pathways.

3.3. $O_2^{2+} + C_2H_4$

In Table 3 the different reaction channels observed following collisions (E_{com} = 4.7 eV) between O_2^{2+} and C_2H_4 are listed. As for the other two collision systems reported in this work, SET is the dominant reactive process accounting for over 80% of the observed product ions. DET accounts for only 4% of the ion yields while 12% of the reactions lead to bond-forming products. The major bond forming channel is 3.1 which leads to $HCO^+ + CH_2^+$. The second most intense reaction is channel 3.4, forming $OH^+ + C_2H_3^+$. There are two other weak bond-forming channels where $CO^+ + H^+$ (channel 3.2) and $C_2OH^+ + H^+$ (channel 3.3) are detected.

3.3.1. Formation of HCO^+

In Fig. 6 the CM frame scattering for HCO^+ and CH_2^+ formed in channel 3.1 is shown. The scattering has a distinct 'forward'

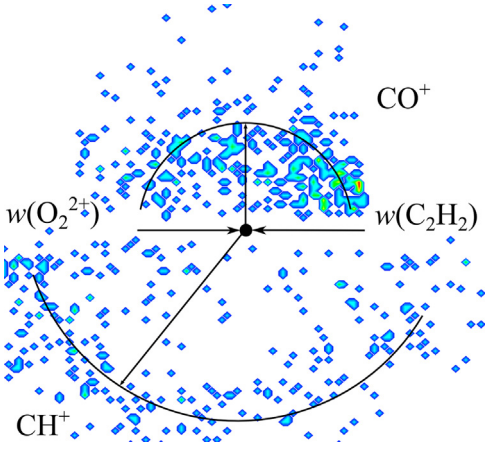

Fig. 5. The CM frame scattering of the $CO^+ + CH^+$ products (channel 2.5) recorded following the reaction of $O_2^{2+} + C_2H_2$ at E_{com} = 4.0 eV. The upper arc marks a CM velocity of 0.3 cm μs^{-1} while the lower arc marks a CM velocity of 0.9 cm μs^{-1}.

Table 3
Observed reaction channels, together with their branching ratios and enthalpies, following the reaction of O_2^{2+} with C_2H_4 at E_{com} = 4.7 eV. Relevant energetics are determined from literature values [39] coupled with the double ionisation energy of O_2 [42].

Channel	Products	Branching ratio	$-\Delta E_T$/eV	ΔH_{lit}/eV[a]
	Single electron transfer	83.7		
	Double electron transfer	4.1		
	Bond forming			
3.1	$HCO^+ + CH_2^+ + [O + H]$	6.4		−8.93[b]
3.2	$CO^+ + H^+ + [C + H + H + O]$	0.4		−0.85
3.3	$C_2OH^+ + H^+ + [O + H + H]$	0.1		[c]
3.4	$OH^+ + C_2H_3^+ + O$	5.3	−6.3	−9.27

[a] All enthalpies are calculated assuming the neutral products are fully atomised.
[b] Enthalpy has been calculated assuming that the product is in the form HCO^+ not COH^+.
[c] No relevant enthalpies of formation are available.

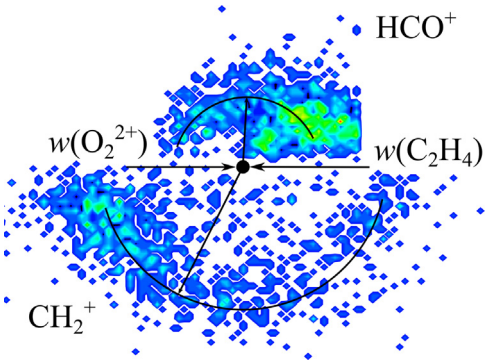

Fig. 6. The CM frame scattering diagram for the formation of $HCO^+ + CH_2^+$ (channel 3.1) following the reaction of $O_2^{2+} + C_2H_4$ at E_{com} = 4.7 eV. The upper arc marks a CM velocity of 0.3 cm μs^{-1} while the lower arc marks a CM velocity of 1.0 cm μs^{-1}.

and 'backward' component. The HCO^+ product is scattered in the same direction as the O_2^{2+} reactant. In contrast the CH_2^+ product is scattered in the same direction as the C_2H_4 reactant. As discussed above, this scattering motif indicates a direct reaction mechanism, which, in turn, implies that the reaction occurs in the following manner: the O_2^{2+} strips a CH_2^- from the C_2H_4 as they move past each other leaving a CH_2^+ product. The nascent $H_2CO_2^{+*}$ subsequently fragments further to give HCO^+ and [H + O].

$$O_2^{2+} + C_2H_4 \rightarrow CH_2^+ + H_2CO_2^{+*}$$
$$\text{then } H_2CO_2^{+*} \rightarrow HCO^+ + [H + O]. \quad (3)$$

It is not possible from our data to definitively determine the form of the neutral products from this reaction. However, if we make the assumption the neutral is OH and generate the internal frame scattering diagrams, all is in accord with the mechanism proposed above. (Eq. (3)). The internal frame scattering diagram clearly indicates that the HCO^+ and OH products have correlated velocities, and those velocities are directed away from that of the CH_2^+ product. As before, we can derive the average velocity of the nascent precursor ion ($H_2CO_2^{+*}$ in this case) and we see that the scattering centre of the HCO^+ and OH velocity vectors, in the internal frame, is clearly centred on this precursor velocity. Thus, the experimental evidence for the mechanism shown in Eq. (3) is consistent and robust.

3.3.2. Formation of OH^+

Interactions of O_2^{2+} with C_2H_4 can form OH^+ (channel 3.4) along with $C_2H_3^+$ and a neutral O atom. As this is a three-body reaction our experimental data can be used to unambiguously extract the velocities of all the products. Fig. 7(a) shows the CM scattering for the $C_2H_3^+$ and OH^+ products while Fig. 7(b) shows the internal frame scattering of OH^+ and O relative to $C_2H_3^+$. Given the analysis presented above, these scattering diagrams clearly show the reaction involves the stripping of a H^- ion from the C_2H_4 by O_2^{2+} to form $C_2H_3^+$ and HO_2^{+*}. The HO_2^{+*} then dissociates, ejecting an O atom, to yield the detected OH^+ product. Again, if this mechanism is correct then it predicts that the products formed from dissociation of the HO_2^{+*} precursor should be scattered around a point in the internal frame scattering diagram that represents the velocity of the HO_2^{+*} precursor. From the modal velocity of the $C_2H_3^+$ product that we determine experimentally (0.64 cm μs^{-1}) we estimate the modal HO_2^{+*} velocity to be 0.52 cm μs^{-1}. This precursor velocity agrees nicely with the scattering centre of the HO^+ and O velocities revealed in Fig. 7(b).

3.4. Comparison of collision systems

All three of these collision systems exhibit a rich and varied bond-forming chemistry. In fact, there are undoubtedly more bond-forming channels in any one of these collision systems than in any other single dication/neutral collision system we have investigated to date. Satisfyingly, there are many similarities in the bond-forming reactivity observed following collisions of O_2^{2+} with the three different organic reactants. For each of the collision systems, the total contribution of the bond-forming channels to the total ion yield is very similar (*ca.* 10%). Additionally, the principal ionic product of the bond-forming reactivity in all three collision

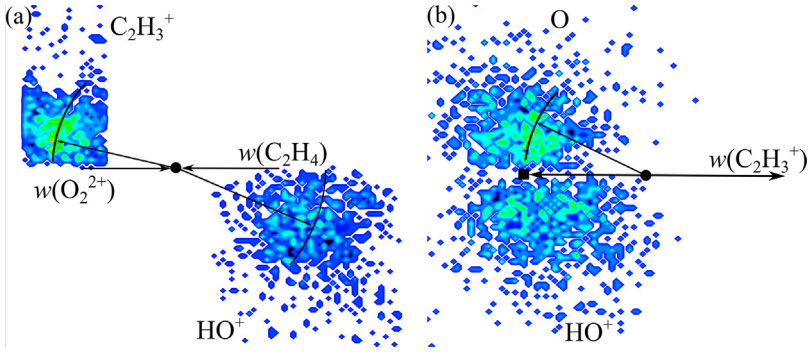

Fig. 7. Scattering diagrams for reaction channels observed following the reaction of $O_2^{2+} + C_2H_4$ at E_{com} = 4.7 eV. (a) The CM frame scattering diagram for the formation of $HO^+ + C_2H_3^+$ products from channel 3.4. The upper arc marks a CM velocity of 0.6 cm μs^{-1} while the lower arc marks a CM velocity of 0.8 cm μs^{-1}. (b) Internal frame scattering diagram for HCO^+ and O relative to CH^+ for channel 3.4. The square marks the velocity of the dissociating precursor HCO_2^{+*} (0.6 cm μs^{-1}).

systems is HCO^+. However, these HCO^+ products are not formed by one common reaction mechanism across the three collision systems. Following the reaction of O_2^{2+} and CH_4, HCO^+ is formed *via* a collision complex. In comparison, in the reactions of O_2^{2+} with C_2H_2 and C_2H_4, HCO^+ is formed by a striping reaction which breaks the carbon—carbon bond in the neutral reactant. Obviously, in the case of reactions with methane there is no C—C bond to break, so an alternative mechanism must necessarily operate.

One difference in the bond-forming reactivity exhibited by the three systems relates to the facility for the stripping of H^- from the organic molecule by O_2^{2+}. This form of reactivity is observed in the reaction of O_2^{2+} with both CH_4 and C_2H_4 but not with C_2H_2. A possible reason for this behaviour is the relative strengths of the C—H bonds in CH_4, C_2H_2 and C_2H_4. A good guideline for the relative ease of hydride donation from the neutral should be the heterolytic dissociation energy of the different neutrals (*e.g.* ΔH for $CH_4 \rightarrow CH_3^+ + H^-$). It is possible to estimate these heterolytic dissociation energies from enthalpies of formation available in the literature; for example, to estimate the heterolytic dissociation energy for CH_4 $\Delta_f H$ is required for CH_4, CH_3^+ and H^- [39,40]. The calculated values of the heterolytic dissociation energies are 13.87 eV, 17.22 eV and 15.14 eV for CH_4, C_2H_2 and C_2H_4 respectively. From these energetic estimates we see that more energy is required to fragment the C—H bond in C_2H_2, to form H^- (and C_2H^+), than to heterolytically cleave the C—H bonds in CH_4 or C_2H_4. These energies indicate that the energetic cost of heterolytically breaking the C—H bond can account for the lack of H^- transfer in the O_2^{2+}/C_2H_2 collision system. Further insight comes from applying a "spectator stripping" model to this hydride transfer reaction [41]. Applying the kinematic constraints of this model, which dictate the final velocities of the products of the hydride transfer, together with the above energetics, reveals that facile hydride transfer in the O_2^{2+}/C_2H_2 collision system is likely to require markedly greater collision energies than in collisions of O_2^{2+} with CH_4 and C_2H_4. Thus, it is not surprising that, at our relatively low collision energies we do not observe hydride transfer in the O_2^{2+}/C_2H_2 collision system.

4. Conclusions

We have studied the reactions of the molecular oxygen dication with three small organic molecules, CH_4, C_2H_2 and C_2H_4, at centre-of-mass collision energies close to 4 eV. The ion yield in all three collision systems is dominated by electron transfer. However, all three systems also show a significant number of bond-forming products; for example HCO^+, CO^+, HO^+, HO_2^+, CO_2^+, C_2O^+ and C_2OH^+ are all detected.

The correlations between the product (ionic and neutral) velocity vectors, which are revealed by our coincidence methodology, provide significant insight into the different mechanisms of these bond-forming processes. Several bond-forming reactions proceed *via* the formation of long-lived collision complexes which subsequently fragment to a pair of monocations. At least one of these nascent monocations then subsequently fragments further. Other bond-forming reactions occur *via* a direct process in which the dication removes an atom (or group of atoms) from the neutral as it flies past, breaking strong chemical bonds.

Acknowledgments

This work was supported by funding from the EPSRC, including a studentship for JFL, and UCL. The authors acknowledge the use of the UCL Legion High Performance Computing Facility (Legion@UCL), and associated support services, in the completion of this work.

Appendix A. Supplementary data

Supplementary data associated with this article can be found, in the online version, at http://dx.doi.org/10.1016/j.ijms.2014.01.014.

References

[1] C. Simon, J. Lilensten, O. Dutuit, R. Thissen, O. Witasse, C. Alcaraz, H. Soldi-Lose, Ann. Geophys. 23 (2005) 781.
[2] C. Nicolas, C. Alcaraz, R. Thissen, J. Zabka, O. Dutuit, Planet. Space Sci. 50 (2002) 877.
[3] R. Thissen, O. Witasse, O. Dutuit, C.S. Wedlund, G. Gronoff, J. Lilensten, Phys. Chem. Chem. Phys. 13 (2011) 18264.
[4] M.A. Parkes, J.F. Lockyear, S.D. Price, Int. J. Mass Spectrom. (2013), http://dx.doi.org/10.1016/j.ijms.2013.06.018 (in press).
[5] M.A. Parkes, J.F. Lockyear, S.D. Price, D. Schröder, J. Roithová, Z. Herman, Phys. Chem. Chem. Phys. 12 (2010) 6233.
[6] B.K. Chatterjee, R. Johnsen, J. Chem. Phys. 91 (1989) 1378.
[7] J. Glosik, A.B. Rakshit, N.D. Twiddy, N.G. Adams, D. Smith, J. Phys. B 11 (1978) 3365.
[8] H. Störi, E. Alge, H. Villinger, F. Egger, W. Lindinger, Int. J. Mass Spectrom. Ion Phys. 30 (1979) 263.
[9] D. Smith, D. Grief, N.G. Adams, Int. J. Mass Spectrom. Ion Phys. 30 (1979) 271.
[10] P. Franceschi, R. Thissen, O. Dutuit, C. Alcaraz, H. Soldi-Lose, D. Bassi, D. Ascenzi, P. Tosi, J. Zabka, Z. Herman, M. Coreno, M.d. Simone, Int. J. Mass Spectrom. 280 (2009) 119.
[11] W. Lindinger, E. Alge, H. Störi, M. Pahl, R.N. Varney, J. Chem. Phys. 67 (1977) 3495.
[12] M.A. Parkes, J.F. Lockyear, S.D. Price, Int. J. Mass Spectrom. 280 (2009) 85.
[13] J. Jašik, J. Roithová, J. Žabka, R. Thissen, I. Ipolyi, Z. Herman, Int. J. Mass Spectrom. 255–256 (2006) 150.
[14] J. Roithová, C. Ricketts, D. Schröder, Int. J. Mass Spectrom. 280 (2009) 32.
[15] C.L. Ricketts, D. Schröder, C. Alcaraz, J. Roithová, Chem. Eur. J. 14 (2008) 4779.
[16] J. Roithová, D. Schröder, J. Am. Chem. Soc. 128 (2006) 4208.
[17] J.C. Weisshaar, Acc. Chem. Res. 26 (1993) 213.
[18] Y.A. Ranasinghe, T.J. MacMahon, B.S. Freiser, J. Am. Chem. Soc. 114 (1992) 9112.
[19] Y.D. Hill, Y.Q. Huang, T. Ast, B.S. Freiser, Rapid Commun. Mass Spectrom. 11 (1997) 148.
[20] S.W. Buckner, B.S. Freiser, J. Am. Chem. Soc. 109 (1987) 1247.
[21] Y.A. Ranasinghe, T.J. MacMahon, B.S. Freiser, J. Phys. Chem. 95 (1991) 7721.
[22] Y.Q. Huang, B.S. Freiser, J. Am. Chem. Soc. 110 (1988) 4434.
[23] E. Di Santo, M. Santos, M.C. Michelini, J. Marçalo, N. Russo, J.K. Gibson, J. Am. Chem. Soc. 133 (2011) 1955.
[24] Z. Herman, Int. Rev. Phys. Chem. 15 (1996) 299.
[25] S.A. Rogers, S.D. Price, S.R. Leone, J. Chem. Phys. 98 (1993) 280.
[26] S.D. Price, J. Chem. Soc. Faraday Trans. 93 (1997) 2451.
[27] S.D. Price, Phys. Chem. Chem. Phys. 5 (2003) 1717.
[28] D. Schroder, H. Schwarz, J. Phys. Chem. A 103 (1999) 7385.
[29] J.F. Lockyear, M.A. Parkes, S.D. Price, Angew. Chem. Int. Ed. 50 (2011) 1322.
[30] S.D. Price, Int. J. Mass Spectrom. 260 (2007) 1.
[31] W.-P. Hu, S.M. Harper, S.D. Price, Meas. Sci. Technol. 13 (2002) 1512.
[32] J.H.D. Eland, Meas. Sci. Technol. 4 (1993) 1522.
[33] A. Oelsner, O. Schmidt, M. Schicketanz, M. Klais, G. Schonhense, V. Mergel, O. Jagutzki, H. Schmidt-Bocking, Rev. Sci. Instrum. 72 (2001) 3968.
[34] J.F. Lockyear, C.L. Ricketts, M.A. Parkes, S.D. Price, Chem. Sci. 2 (2011) 150.
[35] J.F. Lockyear, M.A. Parkes, S.D. Price, J. Phys. B 42 (2009) 145201.
[36] R.D. Levine, R.B. Bernstein, Molecular Reaction Dynamics and Chemical Reactivity, Oxford University Press, Oxford, 1987.
[37] M.A. Parkes, J.F. Lockyear, D. Schroder, J. Roithova, S.D. Price, Phys. Chem. Chem. Phys. 13 (2011) 18386.
[38] M.J. Frisch, G.W. Trucks, H.B. Schlegel, G.E. Scuseria, M.A. Robb, J.R. Cheeseman, G. Scalmani, V. Barone, B. Mennucci, G.A. Petersson, H. Nakatsuji, M. Caricato, X. Li, H.P. Hratchian, A.F. Izmaylov, J. Bloino, G. Zheng, J.L. Sonnenberg, M. Hada, M. Ehara, K. Toyota, R. Fukuda, J. Hasegawa, M. Ishida, T. Nakajima, Y. Honda, O. Kitao, H. Nakai, T. Vreven, J.A. Montgomery Jr., J.E. Peralta, F. Ogliaro, M. Bearpark, J.J. Heyd, E. Brothers, K.N. Kudin, V.N. Staroverov, R. Kobayashi, J. Normand, K. Raghavachari, A. Rendell, J.C. Burant, S.S. Iyengar, J. Tomasi, M. Cossi, N. Rega, J.M. Millam, M. Klene, J.E. Knox, J.B. Cross, V. Bakken, C. Adamo, J. Jaramillo, R. Gomperts, R.E. Stratmann, O. Yazyev, A.J. Austin, R. Cammi, C. Pomelli, J.W. Ochterski, R.L. Martin, K. Morokuma, V.G. Zakrzewski, G.A. Voth, P. Salvador, J.J. Dannenberg, S. Dapprich, A.D. Daniels, Ö. Farkas, J.B. Foresman, J.V. Ortiz, J. Cioslowski, D.J. Fox, Gaussian 09, Gaussian, Inc., Wallingford, CT, 2009.
[39] S. Lias, J. Bartmess, J. Liebman, J. Holmes, R. Levin, W. Mallard, in: W. Mallard, P. Linstrom (Eds.), NIST Chemistry WebBook, NIST Standard Reference Database Number 69, National Institute of Standards and Technology, Gaithersburg, MD, 2013, p. 20899, http://webbook.nist.gov
[40] K.R. Lykke, K.K. Murray, W.C. Lineberger, Phys. Rev. A 43 (1991) 6104.
[41] J.C. Polanyi, J.L. Schreiber, in: W. Jost (Ed.), Physical Chemistry an Advanced Treatise, vol. 6A, Academic Press, London, 1974.
[42] R.I. Hall, G. Dawber, A. McConkey, M.A. Macdonald, G.C. King, Phys. Rev. Lett. 68 (1992) 2751.